

KIAA1530/UVSSA is responsible for UV-sensitive syndrome that facilitates damage-dependent processing of stalled RNA polymerase IIo in TC-NER

Yuka Nakazawa^{1, 2, 3, 16}, Kensaku Sasaki^{4, 16}, Norisato Mitsutake^{1, 3, 16}, Michiko Matsuse^{1, 3}, Mayuko Shimada^{1, 2, 3}, Tiziana Nardo⁵, Yoshito Takahashi⁶, Kaname Ohyama^{1, 7}, Kosei Ito^{1, 8}, Hiroyuki Mishima⁴, Masayo Nomura⁴, Akira Kinoshita^{1, 4}, Shinji Ono⁴, Katsuya Takenaka⁹, Ritsuko Masuyama⁸, Takashi Kudo¹⁰, Hanoch Slor¹¹, Atsushi Utani¹², Satoshi Tateishi¹³, Shunichi Yamashita^{3, 14}, Miria Stefanini⁵, Alan R Lehmann¹⁵, Koh-ichiro Yoshiura⁴ & Tomoo Ogi^{1, 2, 3}

¹Nagasaki University Research Centre for Genomic Instability and Carcinogenesis (NRGIC), Nagasaki, Japan

²Department of Molecular Medicine, Atomic Bomb Disease Institute, Graduate School of Biomedical Sciences, Nagasaki University, Nagasaki, Japan

³Department of Radiation Medical Sciences, Atomic Bomb Disease Institute, Graduate School of Biomedical Sciences, Nagasaki University, Nagasaki, Japan

⁴Department of Human Genetics, Atomic Bomb Disease Institute, Graduate School of Biomedical Sciences, Nagasaki University, Nagasaki, Japan

⁵Istituto di Genetica Molecolare, Consiglio Nazionale delle Ricerche, Pavia, Italy

⁶Innovative Beauty Science Laboratory, Kanebo Cosmetics, Odawara, Japan

⁷Department of Environmental and Pharmaceutical Sciences, Graduate School of Biomedical Sciences, Nagasaki University, Nagasaki, Japan

⁸Department of Cell Biology, Graduate School of Biomedical Sciences, Nagasaki University, Nagasaki, Japan

⁹Department of Molecular Genetics, Medical Research Institute, Tokyo Medical and Dental University, Tokyo, Japan

¹⁰Department of Radioisotope Medicine, Atomic Bomb Disease Institute, Graduate School of Biomedical Sciences, Nagasaki University, Nagasaki, Japan

¹¹Human Molecular Genetics and Biochemistry, Sackler School of Medicine, Tel Aviv University, Tel Aviv, Israel

¹²Department of Dermatology, Graduate School of Biomedical Sciences, Nagasaki University, Nagasaki, Japan

¹³Institute of Molecular Embryology and Genetics, Kumamoto University, Kumamoto, Japan

¹⁴Vice President, Fukushima Medical University, Fukushima, Japan

¹⁵Genome Damage and Stability Centre, University of Sussex, Brighton, United Kingdom

¹⁶These authors contributed equally to this work.

Corresponding author: T.O. (togi@nagasaki-u.ac.jp)

UV-sensitive syndrome (UV^SS) is a genodermatosis characterised by cutaneous photosensitivity without skin-carcinoma¹⁻⁴. Despite the mild clinical features, UV^SS cells, like Cockayne syndrome (CS) cells, are very UV-sensitive and lack of transcription-coupled-NER (TC-NER)^{2,4,5}, a nucleotide excision repair sub-pathway that removes DNA-damage from actively transcribed genes⁶. Three of the seven known UV^SS cases (Supplementary Table 1), are mutated in the CS-responsible *ERCC8* or *ERCC6* (also known as *CSA* and *CSB*, respectively) genes^{7,8}. The remaining four patients form a separate complementation group, UV^SS-A (refs. 1,9,10, and this study); however, the responsible gene, *UVSSA*, has

not yet been identified. Based on exome-sequencing¹¹, we have identified the *UVSSA* gene as *KIAA1530*. *UVSSA* interacts with TC-NER machinery and stabilizes ERCC6-complex; it also facilitates ubiquitination of RNA-polIIo stalled at DNA-damaged sites. Our results provide mechanical insights into the processing of stalled RNA polymerase by *UVSSA* and the CS-complexes, and help to explain the differences in the clinical features of these TC-NER-deficient disorders.

We initially performed exome-sequencing¹¹ of the two UV^SS-A patients, Kps3 and XP24KO (details described in **Methods, Supplementary Note, Table 1, and Supplementary Tables 2a-2c**). Based on a recessive model of inheritance, we directly identified *KIAA1530* (NCBI/Gene-ID: 57654) mapping onto Chr.4p16.3 and encoding a 709aa function-unknown protein as a prime candidate for the disease-responsible gene; later we named it *UVSSA* (**Table 1, Supplementary Table 2c**). The patients were homozygous for c.367A>T mutation in *UVSSA*, which led to a premature termination, p.Lys123* (**Fig. 1a, b**). We identified the same homozygous mutation in Kps2 (sib. of Kps3), and a homozygous c.87delG, causing a frameshift p.Ile31Phefs*9, in an Israeli patient UV^SS24TA (**Fig. 1b, c, Supplementary Note, Supplementary Fig. 1**). The identified mutations are summarized in **Fig. 1d**. We did not detect the 80kDa *UVSSA* protein in any of the UV^SS-A patients (**Fig. 1e**). We additionally examined several mild xeroderma pigmentosum (XP) cases; in one such case, XP70TO¹² (**Supplementary Table 1**), we identified a homozygous p.Cys32Arg, in the *UVSSA* (**Fig. 1c, d**), implying that XP70TO is also in the UV^SS-A group. The mutant protein was stably expressed in XP70TO cells (**Fig. 1f, Supplementary Fig. 2a-d**).

Allele frequencies of the identified mutations in a control population were examined (**Supplementary Note, Supplementary Fig. 3a**). Haploinsufficiency for *UVSSA* is negligible as the parents of Kps2/Kps3 showed no symptoms⁴. In parallel with exome-sequencing, we performed whole-genome SNP-genotyping to identify runs-of-homozygosity (ROH) shared among the patients. We identified three overlapping-ROHs (> 1Mbps) on autosomes, one of which encompasses the *UVSSA* locus (**Fig. 1g, Supplementary Table 3a, b, Supplementary Fig. 3b, c**). No chromosome copy number variation was detected (**Supplementary Fig. 3d**).

The above findings strongly suggest that the mutations in *UVSSA* in the UV^SS-A patients are causal for the disease; we therefore, next examined the NER-activities in the UV^SS-A cells (**Fig. 2**). Unscheduled-DNA-synthesis (UDS¹³, defective in XP) was nearly normal; however, RNA-synthesis-recovery (RRS¹⁴, defective in UV^SS and in CS) was reduced in all cell-strains mutated in *UVSSA* (**Fig. 2a, b**; UDS and RRS were measured using a recently-developed rapid non-radioactive system^{15,16}). Similarly, siRNA-based depletion of the *UVSSA* gene (**Fig. 2c**) caused a drastic reduction of RRS (**Fig. 2d, Supplementary Fig. 4**), whereas UDS was unaffected (**Fig. 2e**). Ectopic-expression of the wild-type *UVSSA* cDNA in UV^SS-A cells restored normal RRS (**Fig. 2f**; V5-tagged-*UVSSA* immunofluorescent-staining shown in **Fig. 2g**), while it did not affect RRS-level in normal, CS-A, or CS-B cells; neither *ERCC8* nor *ERCC6* cDNA expression in UV^SS-A cells restored the RRS-level. We conclude that *KIAA1530/UVSSA* is the causal gene for UV^SS-A.

ERCC8 and *ERCC6* genes are responsible for both CS and UV^SS^{7,8}. To evaluate whether *UVSSA* mutations may also result in CS-phenotypes, we sequenced

the *UVSSA* gene of 61 CS-patients whose genetic defects had not yet been determined (**Supplementary Table 4**). We found no obvious mutations except for four novel heterozygous changes. These changes as well as the SNPs, also found in control and UV^SS-A individuals, do not affect the RRS-activity (**Supplementary Fig. 5**). These data suggest that the *UVSSA* function is distinct from CS-genes (details described in **Supplementary Note**).

Amino-acid sequences of human-*UVSSA* and its orthologues have no obvious similarity to other protein families. A domain of unknown function, DUF2043 (EMBL/EBI-ID: IPR018610) is located near the C-terminus (**Fig. 3a**). We performed a 3D-structure prediction using the PHYRE-server¹⁷ and identified a motif of 143-163aa near to the N-terminus, which had substantial homology with the VHS (Vps-27, Hrs, and STAM) domain¹⁸ (**Fig 3a, Supplementary Fig. 6a, b**). VHS-domain-proteins have been recently implicated in ubiquitin-binding¹⁹. A crystallographic study determined that Trp26 located in the α 2-helix of STAM1 VHS-domain interfaces with ubiquitin-Ile44²⁰ (**Supplementary Fig. 6c**). The *UVSSA*-Cys32 is located in the same α 2-helix (**Supplementary Fig. 6b**); the Cys32Arg mutation is superimposed onto the STAM1/ubiquitin-complex (3D-structure), which indicates that the Arg32 residue is oriented in the same direction as STAM1-Trp26 (**Supplementary Fig. 6d**). These findings suggest that the *UVSSA*-Cys32Arg change occurring in XP70TO may obstruct interactions between the VHS-domain and ubiquitinated proteins.

To investigate the importance of the DUF2043 and VHS-domain in TC-NER, we transduced *UVSSA* truncation-mutants into the UV^SS-A cells and assayed their ability to complement the RRS-defect (**Fig. 3b**). None of the

truncation-mutants lacking either the VHS-domain or DUF2043 was able to restore the RRS-activity of the UV^{SS}-A cells (**Fig. 3c**; **Supplementary Fig. 7a**; Note that T1 and T3 were unstable, **Supplementary Fig. 7b**). Next, we mutated residues conserved from human to Nematoda (**Fig. 3d**, **Supplementary Fig. 8**); we found that out of the 32, only the three located in the VHS-domain (Cys32Arg, Trp120Ala, and Arg157Lys158Arg159GluGluGlu) failed to restore normal RRS-levels (**Fig. 3e**; **Supplementary Fig. 9**). Although we could not determine the critical amino-acid residues responsible for the DUF2043 function, overall these findings indicate that the ubiquitin-binding VHS-domain and DUF2043 of UVSSA are crucial for their TC-NER activity.

We next examined the association of UVSSA with TC-NER factors by immunoprecipitation. UVSSA interacted with several subunits of the core-TFIIH (ERCC3/XPB-p89, ERCC2/XPD, and GTF2H1/p62), and CAK (cdk7, cyclin H, and MAT1) sub-complexes, with the ERCC6, and with the XPA-binding-protein XAB2; no robust interaction was observed between UVSSA and ERCC5 (also known as XPG) (**Fig. 3f**). Similar interactions were also observed after UV-irradiation (**Fig. 3g**). UVSSA is thus a novel factor associated with the TC-NER complexes. The absence of ERCC5 protein in the TFIIH/UVSSA complex appears to conflict with a report demonstrating that ERCC5 is important for stabilizing TFIIH²¹; this could be partially explained by an assumption that ERCC5 and UVSSA may share the same binding-interface of TFIIH.

In unirradiated cells, the UVSSA binding capabilities were unaffected by mutations in the VHS-domain (**Fig. 3f**, lane 6, **Supplementary Fig. 10a**, lane 6). However, following UV-irradiation, interactions with some TFIIH-subunits, namely

GTF2H1 and ERCC3, and with ERCC6, were substantially weakened by the VHS-domain amino-acid substitutions (**Fig. 3g**, lane 6, **Supplementary Fig. 10b**, lane 6). These interactions were confirmed by reverse-immunoprecipitation (**Supplementary Fig. 10c**). These data indicate that UVSSA interacts transiently with the NER-machinery and the VHS-domain specifically supports its direct contacts with TFIIF-core complex and ERCC6 after UV-irradiation.

In TC-NER, the stalled RNA polymerase II (RNA-polII) has first to be displaced by backtracking or degradation to allow access of the NER-machinery⁶. ERCC8/ERCC6-complexes (CS-complexes) are essential for these processes²². During this process, some of the elongating form of RNA-polII (RNA-polIIo), which is phosphorylated (Ser2, and Ser5) in the C-terminal domain (CTD), is ubiquitinated²³, although the precise function and importance of the ubiquitination is obscure. We compared RNA-polIIo modifications after UV-irradiation in the presence of cycloheximide (CHX) in normal, CS, and UV^SS-A cells (**Fig. 4a**; TC-NER activity was unaffected by CHX in the experimental conditions we used, **Supplementary Fig. 11**). In normal cells (**Fig. 4a**, lanes 1-8), a slow-migrating fraction of RNA-polIIo was observed after UV-irradiation and this modified band (form 3) subsequently decreased in intensity. The form 3 was not detected in normal cells upon induction of oxidative-DNA-damage by treatment with hydrogen peroxide (**Supplementary Fig. 12**), suggesting that the modification is UV-damage specific event. We confirmed that this RNA-polIIo modification was ubiquitination as reported previously²³ (**Fig. 4b**). In contrast in the UV^SS cells, the ubiquitinated band was barely detectable, but a fast-migrating form of RNA-polIIo (form 1) was observed and subsequently the normally-migrating form 2 decreased in intensity over the 6-hour period (**Fig. 4a**,

lanes 9-24). In the CS2AW (CS-A) or CS10LO (CS-B) cells (**Fig. 4a**, lanes 25-32), neither ubiquitination (see also ref. 23) nor form 1 was detected. Transduction of wild-type *UVSSA* cDNA into UV^SS-A cells Kps3 restored the ubiquitination of RNA-polIIo following UV-irradiation (**Fig. 4c**, H5-antibody, lanes 5-8). *UVSSA* overexpression was also associated with a substantial reduction of form 1 after UV-irradiation (compare bands in **Fig. 4c**, H5-antibody, lanes 5-8 and 1-4; see also **Fig. 4c**, N20-antibody, and its lanes 1-4, which are shown as a stretched picture on the right-hand).

During transcription, RNA-polIIo is eventually dephosphorylated to RNA-polIIa, for recycling of RNA-polIII for another round of transcription initiation. In TC-NER, displaced RNA-polIIo is also dephosphorylated and recycled (**Fig. 4c**, N20-antibody, lanes 9-12). The dephosphorylation was substantially inhibited in UV^SS-A cells 4-6 h after UV-irradiation (**Fig. 4c**, N20-antibody, lanes 1-4), as previously reported for CS cells²⁴, and was restored following expression of the *UVSSA* cDNA (**Fig. 4c**, N20-antibody, lanes 5-8). The RNA-polIIo ubiquitination was not restored in Kps3 cells by expression of the VHS-domain amino-acid substitution mutants (**Fig. 4d**, H5-antibody, lanes 9-12; **Supplementary Fig. 13**, H5-antibody, lanes 9-12), indicating that the VHS-domain is crucial for the RNA-polIIo processing.

We noticed that ERCC6 protein was degraded in UV^SS-A cells after UV-irradiation, indicating that *UVSSA* contributes to the stabilization of ERCC6-complex in TC-NER process (**Fig. 4d**, ERCC6, lanes 1-4). The reduction of ERCC6 protein-level in Kps3 cells was restored following expression of either the wild-type- or VHS-domain mutated- (Cys32Arg) *UVSSA* (**Fig. 4d**, ERCC6, lanes 5-12; **Supplementary Fig. 14**). These data indicate that the lack of RNA-polIIo ubiquitination in the UV^SS-A cells is not a side effect of CS-protein depletion (see

also **Fig. 2f**, ectopic-expression of *ERCC6* did not restore the RRS-level in UV^SS-A cells). We further showed that the UVSSA specifically binds to RNA-polIIo and ubiquitinated-RNA-polIIo, but not RNA-polIIa, and that the ubiquitinated-RNA-polIIo is enriched in the UVSSA-binding-fraction (**Fig. 4e**).

These findings suggest that UVSSA recruits an E3-ubiquitin-ligase and facilitates ubiquitination of RNA-polIIo. K48-linked-polyubiquitination triggers 26S-proteasomal degradation of the targeted protein, whereas mono- and K63-linked-poly- ubiquitinations contribute to functional modifications. BRCA1/BARD1-complex and NEDD4 E3-ubiquitin-ligases as well as ERCC8-complex have been reported to be involved in damage-dependent polyubiquitination and degradation of RNA-polIIo²⁵⁻²⁷. To determine whether RNA-polIIo is degraded as a consequence of UVSSA-mediated ubiquitination, we analyzed RNA-polIIo modifications after UV-irradiation followed by treatment with a 26S-proteasomal inhibitor, MG132, in normal, and UV^SS-A cells (**Fig. 4f**). The ubiquitinated form 3 of RNA-polIIo band did not increase substantially in its intensity in normal cells treated with MG132 (compare bands in **Fig. 4f**, H5-antibody, lanes 1-4 and 5-8); conversely, increases of the normal form 2 of RNA-polIIo as well as RNA-polIIa bands were observed both in normal and UV^SS-A cells in the presence of inhibitor (**Fig. 4f**, lanes 5-8, and 13-16). Taken together, these data and **Fig. 4a** indicate that the UVSSA-dependent RNA-polIIo ubiquitination is not subject to 26S-proteasomal degradation and may therefore be K63-linked, although a substantial amount of stalled RNA-polIIo is degraded by the aforementioned UVSSA-independent ubiquitination pathways. We speculate that the TFIIH-core factor, GTF2H2 (p44), is a candidate for the alternative E3-ubiquitin-ligase²⁸, which may form stable K63-linked-poly-ubiquitin chains on stalled RNA-polIIo in TC-NER.

Further studies will address this hypothesis. We conclude that UVSSA plays an important role in the processing of RNA-polII molecules stalled at sites of UV-damage.

In conclusion, we identified a novel gene causing UV-sensitive syndrome, *UVSSA/KIAA1530*, which is involved in TC-NER of UV-damage. UVSSA interacts with TFIIH, ERCC6, and RNA-polIIo and the VHS-domain is indispensable for TC-NER activity and for ubiquitination and dephosphorylation roles in the processing of stalled RNA-polIIo. We hypothesize that UVSSA directly recruits TFIIH at sites where RNA-polIIo is stalled at UV-damage (but not at oxidative-damage: **Supplementary Fig. 12**; see also refs. 5,7,29), and facilitates RNA-polIIo ubiquitination and promotes its backtracking to allow access to the NER-machinery. We also found that UVSSA contributes to stabilization of ERCC6-complex; in the accompanying reports (Zhang *et al.*; Schwertman *et al.*), UVSSA/USP7-complex is shown to be involved in the regulation of ERCC6 ubiquitination. These various UVSSA functions coordinate the removal of stalled RNA-polIIo and formation of the TC-NER pre-incision complex to promote the subsequent steps of NER and transcription resumption at UV-damaged sites.

CS but not UV^SS cells are sensitive to oxidative-DNA-damage^{5,7,29,30}; this differential sensitivity could explain the difference between symptoms in CS and UV^SS. Our findings, however, suggest that aberrant RNA-polIIo may also contribute to the clinical outcome (**Supplementary Fig. 15**). RNA-polIIo stalled at DNA-damage is normally stably-ubiquitinated and backtracked in a process dependent on the CS-complexes and UVSSA, facilitating removal of DNA-damage and prompt transcription resumption (**Supplementary Fig. 15a-d**). In UV^SS-A cells,

stalled RNA-polIIo can be still ubiquitinated in an alternative CS-complexes-dependent, but UVSSA-independent pathway, that leads to 26S-proteasomal degradation of RNA-polIIo, so that transcription resumption do not occur (**Supplementary Fig. 15e, f**). In CS-patients, neither of these pathways is operative (**Supplementary Fig. 15h**), suggesting that prolonged arrest of RNA-polIIo at DNA-lesions (it leads to a signal for apoptosis; see ref. 6 and refs. therein), as in CS cells, is more deleterious than degradation as occurs in UV^S-A cells, and this might contribute to the more severe clinical features in CS than in UV^S. UVSSA is thus a key factor that controls the fate of RNA-polIIo stalled at DNA damage.

URLs. NRGIC, <http://www.nrgic.prj.nagasaki-u.ac.jp/>; NCBI, <http://www.ncbi.nlm.nih.gov/>; EMBL-EBI database, <http://www.ebi.ac.uk/embl/>; PHYRE web-server, <http://www.sbg.bio.ic.ac.uk/phyre/html/index.html>; Picard version 1.38, <http://picard.sourceforge.net/index.shtml>; UCSC, <http://genome.ucsc.edu/>; dbSNP build 131, <http://www.ncbi.nlm.nih.gov/projects/SNP/>; 1000 Genomes project full phase 1 data, <http://www.1000genomes.org/home/>; ANNOVAR-SIFT database, <http://www.openbioinformatics.org/annovar/>.

ACKNOWLEDGEMENTS

We are grateful to Drs. Philip Hanawalt and Graciela Spivak for their helpful comments on the manuscript. We are grateful to Mses Chisa Hayashida, Maiko Kawamichi, and Heather Fawcett for technical assistance. This work was supported by Special Coordination Funds for Promoting Science and Technology from Japan Science and Technology Agency (JST) to Y.N., K.O., K.I., R.M., and T.O.;

a Grant in aid for Scientific Research KAKENHI (22710056) from Japan Society for the Promotion of Science, a science research grant from Inamori Foundation, a cancer research grant from The Sagawa Foundation for Promotion of Cancer Research, a medical research grant from Mochida Memorial Founds for Medical and Pharmaceutical Research, a medical research grant from Daiichi-Sankyo Foundation of Life Science, a medical research grant from Takeda Science Foundation, and a Grant in aid for Seeds Innovation (Type-A) from JST to T.O.; a Global COE Program from the Ministry of Education, Culture, Sports, Sciences and Technology of Japan to Y.N., K.S., N.M., M.M., Mayuko S., S.Y., K.Y., and T.O.; the Associazione Italiana per la Ricerca sul Cancro to Miria S.; an MRC programme grant, and an EC-RTN and integrated project to A.R. L.

AUTHOR CONTRIBUTIONS

N.M. and T.O. designed the study and experiments. Y.N., N.M., M.M., Mayuko S., T.N., K.O., K.I., K.T., R.M., and T.O. performed molecular and cell biological experiments. Y.N., K.S., Mayuko S., Y.T., M.N., A.K., S.O., K.Y., and T.O. performed genetic experiments. K.S., Mayuko S., Y.T., H.M., M.N., A.K., S.O., K.Y., and T.O. analyzed the genetic data. Y.T., H.S., A.U., S.T., Miria S., and A.R.L. contributed CS- and UV^SS- patient materials. N.M., Y.T., T.K., A.U., S.Y., Miria S., A.R.L., and T.O. coordinated the study. N.M., Miria S., A.R.L., and T.O. wrote the manuscript. M.M., Mayuko S., T.N., and Y.T. contributed equally to the study. Miria S., A.R.L., and K.Y. contributed equally to the study. All authors commented on the manuscript.

COMPETING FINANCIAL INTERESTS

The authors declare no competing financial interests.

FIGURE LEGEND

Figure 1 Identification of truncation mutations in the *KIAA1530/UVSSA* gene in UV^SS-A patients. **(a)** Illustration of the c.367A>T mutation causing the p.Lys123* premature stop-mutation, identified in the UV^SS-A patient Kps3. Exome-sequencing data was aligned and individual reads are shown as beige lines; the position of the A>T base substitution is shown in red. **(b)** Capillary Sanger-sequencing showed that UV^SS-A patients XP24KO and Kps3 are homozygous for the c.367A>T single nucleotide variant (SNV) in the *UVSSA* exon 3; the same mutation was also found in the Kps3 sibling, Kps2. The altered amino acid, lysine residue 123 is shown in red (*). **(c)** The c.87delG frameshift mutation and the p.Cys32Arg missense mutation were identified in the UV^SS-A patients UV^SS24TA and in XP70TO, respectively. Electropherograms of the *UVSSA* exon 2 (upper case letters) and intron 2 (lower case letters) are shown. The deletion in the third position of the lysine codon 29 leads to the premature termination, p.Ile31Phefs*9; the transition in the first position of the cysteine codon 32 leads to the p.Cys32Arg change (shown in red). Arrowheads indicate the position where the mutation occurred. **(d)** The genomic structure of the *KIAA1530/UVSSA* gene and the positions of the alterations found in the UV^SS-A patients. **(e, f)** Immunoblots showing the 80kDa *UVSSA* gene product in normal and CS cells, which is **(e)** missing, or **(f)** reduced in the UV^SS-A cells analyzed. ERCC3 (XPB) is a loading control. 48BR and 1BR, normal; CS2AW, CS-A; CS10LO, CS-B; Kps2, Kps3, UV^SS24TA, XP24KO and XP70TO, UV^SS-A cells. Asterisks indicate non-specific bands. **(g)** Shared run-of-homozygous (ROH) segments between the UV^SS-A patients, XP24KO, Kps3, Kps2 and UV^SS24TA. ROHs overlapping in all

four patients are shown as blue bars, and the overlapping region that contains the *UVSSA* gene is shown as a red bar (see **Supplementary Fig. 3b** for ROHs identified in the individual patient; see **Supplementary Fig. 3c** for a magnified view of the overlapped region found in chromosome 4).

Figure 2 RNA synthesis recovery after UV-irradiation requires the *UVSSA* gene expression. **(a)** RRS-levels after UV-irradiation were reduced in the UV^SS-A cells (closed bars, 10J/m² 254nm UVC; open bars, no UV). **(b)** Close to normal UDS-levels in the UV^SS-A cells (closed bars, 20J/m² UVC; open bars, no UV). **(c)** The *UVSSA* gene expression was diminished by small-RNA interference (siRNA). Normal 48BR cells were mock siRNA transfected, or transfected with siRNA targeting the *UVSSA*. The knockdown efficiency, as detected by immunoblotting of the *UVSSA* protein. ERCC3 (XPB) is a loading control. Asterisk indicates a non-specific band. **(d)** RNA synthesis recovery after UV irradiation was completely abolished by abrogation of the *UVSSA* gene expression. Normal 48BR cells were mock siRNA transfected, or transfected with siRNA targeting the *UVSSA* or *XPA* genes (closed bars, 10J/m² UVC; open bars, no UV). **(e)** UDS-level was unaffected by siRNA knockdown of the *UVSSA* expression (closed bars, 20J/m² UVC). **(f)** Ectopic-expression of wild-type *UVSSA* cDNA in the UV^SS-A cells by a recombinant lentivirus infection completely restored the RRS-deficiency (closed bars, 10J/m² UVC; open bars, no UV). Infection efficiencies of the viruses (> 85%) were confirmed by immunofluorescent-staining of V5-tagged-*UVSSA* protein in **g**. RRS-levels were normalised against the RRS-levels in unirradiated cells (**a**, **d**, **f**). UDS-levels were normalised against the UDS-levels of normal 48BR cells (**b**), or of the cells with mock siRNA treated (**e**). Error bars represent standard deviations of

medians of nuclear fluorescence measurements in quintuplicate samples (**a, b, d-f**). 48BR and 1BR, normal; Kps2, Kps3, UV^SS24TA, XP24KO and XP70TO, UV^SS-A; CS2AW, CS-A; CS10LO, CS-B; XP15BR, XP-A cells. (**g**) Ectopically expressed UVSSA protein in the UV^SS-A cells was detected with mouse anti-V5 antibody (green). DAPI, DAPI stain (blue); merge, merged picture. Scale bar, 20 μ m.

Figure 3 N-terminal VHS-domain of the UVSSA protein is essential for RRS-activity and TFIIH interaction. (**a, b**) Schematic representation of the (**a**) human full-length UVSSA, and (**b**) UVSSA truncation mutants used for the RRS-assay in **c**. VHS, tertiary-structure of the N-terminal part of the UVSSA protein shares homology with VHS (Vps-27, Hrs, and STAM) domain; DUF2043, a conserved domain of unknown function (IPR018610, EMBL-EBI); NLS1 and NLS2, putative nuclear localization signals; T1-6, truncation mutants; in T1, and T3, SV40 nuclear localization signal (PKKKRKV) was added to the C-terminal of the mutants. (**c**) RRS-levels were measured in Kps3 cells expressing intact (full) or truncated form (truncation T1-T6) of the V5-tagged UVSSA cDNA (closed bars, 10J/m² UVC; open bars, no UV). (**d**) Schematic representation of the UVSSA amino-acid substitution mutants, which were used for the RRS-assays in **e**, and **Supplementary Fig. 5**. Heterozygous mutations identified in CS-patients are shown in blue (see details in **Supplementary Table 4**); nonsynonymous SNPs found in normal control individuals are shown in orange; mutations shown in black and red are the amino acid substitutions designed for the residues conserved through human to Nematoda as well as the XP70TO disease-causative mutation, p.Cys32Arg. The three mutants shown in red did not complement the RRS-deficiency of Kps3 cells in **e**. (**e**) RRS-levels were measured in Kps3 cells expressing UVSSA amino-acid substitution mutants (closed bars, 10J/m²

UVC; open bars, no UV). Expression of the wild-type, or the mutant UVSSA in Kps3 cells was confirmed by immunofluorescent-staining of V5-tagged proteins (transfection efficiencies were > 85%, see **Supplementary Figs. 7a-b, and 9**). RRS-levels were normalized against the RRS-levels in unirradiated cells (**c, e**). Error bars represent standard deviations of medians of nuclear fluorescence measurements in quintuplicate samples (**c, e**). (**f, g**) The wild-type and Cys32Arg-mutated UVSSA protein interactions with NER-factors were assayed by immunoprecipitation (**f**) without or (**g**) 1 h after 10J/m² UV-irradiation. Interactions were detected by immunoblotting with antibodies against V5-tag (UVSSA), core-TFIIH (ERCC3, ERCC2, and GTF2H1), CAK (cdk7, cyclin H, and MAT1) components, and ERCC6, XAB2, and ERCC5. CL, crude lysate (33% load); IP, immunoprecipitate. The intensities of the bands corresponding to factors binding to the mutant proteins are expressed as percentages of those of the wild type protein. Asterisks indicate non-specific bands.

Figure 4 The UVSSA VHS-domain is essential for the processing of RNA-polIIo. (**a**) RNA-polIIo modification after UV-irradiation in normal (48BR, 1BR), UV^SS-A (Kps3, XP24KO, UV^SS24TA, XP70TO), CS-A (CS2AW), and CS-B (CS10LO) cells (10J/m² UVC, with 100μM cycloheximide). H5-antibody (reacts with the hyper-phosphorylated CTD-Ser2/5) was used to detect the elongating form of RNA-polII (RNA-polIIo). ERCC3 is a loading control. The modified (slow-migrating) form of RNA-polIIo (form 3), and normal- (form 2) and fast- (form 1) migrating RNA-polIIo are indicated. (**b**) Ubiquitination of RNA-polIIo was confirmed by his-ubiquitin pull-down assay. Ubiquitinated RNA-polIIo was detected by H5-antibody. (**c, d**) Lack of RNA-polIIo ubiquitination and dephosphorylation in

Kps3 cells were rescued by expression of the (c) wild-type UVSSA protein but not by (d) the VHS-domain Cys32Arg mutant. Hyper-phosphorylated RNA-polIIo, and hypo-phosphorylated RNA-polIIa were both detected by N20-antibody. Asterisk indicates non-specific band. (e) The UVSSA protein interaction with ubiquitinated RNA-polIIo was assayed by immunoprecipitation. Different forms of RNA-polII species were detected by N20-antibody. (f) Ubiquitinated RNA-polIIo in normal cells is not subject to 26S-proteasomal degradation. Normal (48BR), and UV^SS-A (Kps3) cells were pretreated with or without 12.6 μ M MG-132 as well as CHX 1h prior to 10J/m² UVC irradiation. Ubiquitinated RNA-polIIo was detected by H5-antibody.

Table 1 Direct identification of the UV^SS-A causal gene by exome-sequencing of patients Kps3 and XP24KO.

Filter	Kps3	XP24KO
Single nucleotide variants (SNVs)		
Total SNVs identified	75,368	94,628
non-synonymous missense / stopgain / stoploss / splice site* variants	7,161	6,904
not reported in dbSNP131	383	340
not reported in dbSNP131, 1000GP**	231	210
not reported in dbSNP131, 1000GP**, 7 control exomes*** (novel functionally significant SNVs)	217	202
Insertion and deletions (indels)		
Total indels identified	15,966	19,665
frameshift indels / in-frame stopgain / in-frame stoploss / splice site* variants	327	307
not reported in dbSNP131	198	172
not reported in dbSNP131, 1000GP**	85	76
not reported in dbSNP131, 1000GP**, 7 control exomes*** (novel functionally significant indels)	46	41
Novel functionally significant variants		
novel SNVs / novel indels	263	243
Candidate genes under a recessive model		
homozygous	9	17
compound heterozygous	9	6
Potential causative genes shared among the patients****	1 (KIAA1530/UVSSA)	

The number of variants or genes that meet the left criteria is indicated for each patient. * splice site, splice-site acceptor or donor variants within 6-bp away from exon/intron boundaries; ** 1000GP, 1000 Genomes Project full phase 1, March 2010; *** 7 control exomes, 7 Japanese in-house exome sequencing data; **** Under a recessive model, only a single candidate gene, *KIAA1530/UVSSA*, was identified.

ONLINE METHODS

Human studies. Patient and control samples were obtained with local ethical approval (Nagasaki University ELSI committee).

Exome sequencing. Genomic DNA of the patients (Kps3 and XP24KO) was enriched using the Agilent SureSelect Human All Exon Kit (Agilent, G3362) according to the manufacturer's instructions (Agilent, Santa Clara, CA, USA). The kit covers 1.22% of human genomic regions, which correspond to the CCDS exons. Simply, genomic DNA was fragmented (150~200 bp), and ligated to the Illumina sequencing adaptor oligo nucleotides. The adaptor-ligated fragments were then amplified by ligation-mediated PCR (LM-PCR), followed by hybridization to the SureSelect Biotinylated RNA library for exon enrichment. The hybridized fragments were captured by streptavidin-coated magnetic beads. The captured genomic fragments were sequenced on a single lane of the Illumina Genome Analyzer IIx (GAIIx) sequencer (Illumina, San Diego CA, USA) using 75 bp paired-end reads.

Bioinformatic analysis for the exome data. Low quality sequences of each read-end were filtered out (**Supplementary Table 2a**). In this study, low quality sequences are defined as reads that contain more than six Ns, >40 continuous identical bases, or those contaminated by adaptor sequences during capturing and sequencing steps. The filtered-sequences were aligned to the human reference genome (GRCh37/hg19) with the Burrows-Wheeler Aligner (BWA) version 0.5.8³¹ (**Supplementary Table 2a**). Picard version 1.38 was used to convert, to sort, and to index the aligned data files. Picard was also used to identify and to remove duplicate reads from the samples. Base

quality scores were recalibrated, and sequence reads were locally realigned with the Genome Analysis Toolkit (GATK) version 1.0.4905^{32,33}. Single nucleotide variants (SNVs) were identified by the GATK's 'Unified Genotyper' program (**Supplementary Table 2b**). Low quality variants were then filtered out using the GATK's 'Variant Filtration Walker' tools according to the following criteria: (1) The SNVs cluster and proximity to indels, (2) Confidence (QUAL) score is < 30 , (3) Greater than 10% of aligned reads at a site have mapping quality 0 (MAPQ0), (4) Strand bias (SB) score is > -0.1 , (5) Quality over depth (QD) score is < 5 , or (6) Largest contiguous homopolymer run of variant allele in either direction (HRun) is > 5 . Small insertion and deletions (indels) were detected with the Dindel (detection of indels) program according to the basic procedure for calling indels from a diploid sample in Dindel user guide version 1.0³⁴. We filtered out any indels matching the following criteria: (1) Quality score is < 20 , (2) Reference homopolymer length is > 10 , or (3) Indels allele is not covered by at least one read on both strands. All the variants were annotated with ANNOVAR³⁵. Annotations of variants are based on The National Center for Biotechnology Information (NCBI) and The University of California Santa Cruz (UCSC) databases. Variants identified in the following SNP data bases were removed: the Single Nucleotide Polymorphism Database (dbSNP, build 131); the 1000 Genomes project full phase 1 data that are based on variants from 629 individuals; 7 in-house Japanese exome sequencing data (**Table 1**). The effect of mutation was predicted using Sorting Intolerant from Tolerant (SIFT) score³⁶ (**Supplementary Table 2c**). We obtained SIFT score from the ANNOVAR-SIFT database. According to a recessive inheritance model, we picked-up genes that carried at least one novel homozygous, or more than two heterozygous changes in one gene locus (**Table 1**). See also **Supplementary Note** in details.

Run of homozygosity (ROH) analysis. Whole-genome SNP-genotyping of the UV^SS-A patients was performed on the Genome-Wide Human SNP Array 6.0 (Affymetrix), according to the manufacturer's instruction. The genotype data were generated using the 'birdseed v2 algorithm' in the Genotyping Console 4.0 (Affymetrix). Homozygosity mapping and copy number analysis were performed by the Partek Genomics Suite v6.5 (Partek). We determined the runs of homozygosity (ROHs) of at least 1Mbp, allowing up to 1% errors. The shared ROHs among the patients were identified. Genomic positions of the identified SNPs were based on the human genome (GRCh37/hg19).

Quantitative real-time PCR (qRT-PCR) analysis. Patients' mRNAs were purified using RNeasy mini kit (*QIAGEN*). cDNAs were synthesized from the patients' mRNA using a mixture of oligo-dT and random hexamer primers and SuperScript II reverse transcription system (*Invitrogen*). *UVSSA* mRNA transcript levels in 48BR, Kps3, and XP70TO cells were determined by q-RT-PCR assay using *SYBR Premix Ex-Taq II* polymerase (Perfect Real Time system, TaKaRa Co. Ltd.) and *Thermal Cycler Dice Real Time System II* (TaKaRa Co. Ltd.). Transcripts from the *HPRT1* allele were used as a quantification control. Experiments were triplicated and the qPCR results were analyzed by $\Delta\Delta\text{CT}$ method. qPCR primers used for the assay can be obtained from the companies web site.

High Resolution Melting analysis (HRMA) analysis. HRMA of the *UVSSA* exon 2 and exon 3 in 576 unrelated Japanese control individuals (in house) were performed to determine the allele frequencies of the stop-gain SNVs, p.Lys123* and

p.Ile31Phefs*9, identified in the UV^SS-A patients. HRMA profile was collected on the LightCycler 480 Real-Time PCR system (*Roche*). The melting curves were analyzed by LightCycler 480 Gene Scanning software (*Roche*).

Recovery of RNA Synthesis (RRS) assay. Experimental details have been described previously¹⁶. Cells were plated in plastic 96-well plates. Virus infection was performed 48 h prior to the RRS assay. Cells were UV irradiated (10J/m² 254nm UVC) and incubated for 12 h for RNA synthesis recovery. RRS levels were measured by the fluorescence-based ethynyluridine (EU)-incorporation assay¹⁶. Briefly, recovered cells were incubated for 2 h in media supplemented with 100μM 5-ethynyluridine (EU) followed by EU detection by copper-catalysed fluorescent-azide conjugation reaction (Click-reaction): Cells were fixed and permeabilised in 2% paraformaldehyde, 0.5% triton X-100 in PBS; after washing with PBS, cells were incubated with 15 μM Alexa Fluor 488 azide (Invitrogen) in 50mM Tris-HCl (pH 7.3), 4mM CuSO₄, 10mM sodium ascorbate, and 20ng/ml DAPI for 60 min, followed by washing with PBST (0.05% Tween20). Nuclear fluorescent image acquisition and data processing were automated using GE's *In-Cell-Analyzer* system.

Unscheduled DNA Synthesis (UDS) assay. Experimental details have been described previously^{15,16}. Cells were plated in 96 well plates. siRNA transfection was performed 72 h prior to the UDS assay. UDS levels were measured by the fluorescence-based ethynyldeoxyuridine (EdU)-incorporation assay^{15,16}. Cells were UV-irradiated (20J/m² 254nm UVC) and incubated for 4 h in media supplemented with 5μM 5-ethynyl-2'-deoxyuridine (EdU). Incorporated EdU was detection by copper-catalysed fluorescent-azide conjugation reaction (Click-reaction) as described

above. Nuclear fluorescent image acquisition and data processing were automated using GE's *In-Cell-Analyzer* system.

Immunofluorescence detection of the UVSSA proteins. Cells were plated in glass-bottomed 96-well plates. Lentivirus particles that express either the wild-type or series of mutant UVSSA proteins (V5-tagged) were infected 48 h prior to the immunodetection. Cells were fixed and permeabilized in 2% paraformaldehyde, and 0.2% triton X-100 in PBS; after washing with PBS, cells were incubated with mouse-anti-V5 antibody diluted 1:200 in PBST (0.05% Tween 20) for 1 h, followed by extensive washing with PBST. The cells stained with primary antibody were then incubated for 1h with DAPI (5ng /ml) and 1:1000 diluted rabbit anti-mouse IgG antibody conjugated with Alexa fluor 488 fluorescent dye (Molecular Probes), followed by washing with PBST. Photographs of the cells were captured with an AxioObserver Z1 microscope (Zeiss) equipped with a CCD camera; captured images were analyzed with Axiovision software (Zeiss).

Co-immunoprecipitation. To investigate the interaction of the UVSSA protein with TC-NER factors, HEK293T cells were transfected with the V5-tagged *UVSSA* cDNA expressing plasmids (wild type, Cys32Arg and Trp120Ala mutants), followed by 24h incubation. In the reverse-immunoprecipitation experiments, V5-tagged human cDNAs encoding the *ERCC3* (*XPB*), *GTF2H1* (p62), *CDK7*, *ERCC6* (*CSB*), and *ERCC5* (*XPG*) genes were used. Whole cell lysates were prepared using CellLytic Nuclear Extraction Kit (Sigma). Co-immunoprecipitation was performed using rabbit anti-V5 antibody-conjugated agarose beads (MBL).

Immunoblotting. Whole cell lysates (CL) and immunoprecipitated samples (IP) were resolved by SDS-PAGE (5-20% gradient-gel). Resolved protein samples were transferred to PVDF membrane for immunodetection unless otherwise noted.

Antibodies. Antibodies used for this study were as follows: rabbit polyclonal anti-UVSSA antibody was raised against the N-terminal VHS domain of human UVSSA protein (Gene Tex); mouse polyclonal anti-UVSSA antibody was raised against the full-length of human UVSSA protein (Abnova); mouse monoclonal anti-V5-tag, 1H6 (MBL); rabbit polyclonal anti-V5-tag, PM003 (MBL); mouse monoclonal anti-p89/ERCC3, AB3 (CRUK); rabbit polyclonal anti-p89/ERCC3, S-19 (Santa Cruz); mouse monoclonal anti-XPD/ERCC2, 2F6 (CRUK); mouse monoclonal anti-p62/GTF2H1, G10 (Santa Cruz); mouse monoclonal anti-cdk7, MO1 (MBL); rabbit polyclonal anti-MAT1, FL-309 (Santa Cruz); mouse monoclonal anti-cyclin H, 1B8 (Abnova); mouse monoclonal anti-CSB/ERCC6, 553C5a (BMR); mouse monoclonal anti-XAB2, 5-17 (Santa Cruz); mouse monoclonal anti-XPG/ERCC5, 8H7 (CRUK); mouse monoclonal anti-RNA polymerase II large subunit C-terminal domain Ser-2 phosphorylated, H5 (Covance); rabbit polyclonal anti-RNA polymerase II, N20 (Santa Cruz); rabbit polyclonal anti-phospho-Ser15-p53 (CST).

Detection of the elongating form of RNA polymerase II (RNA polIIo) after UV irradiation. Cells were cultured in media supplemented with 100 μ M cycloheximide (CHX) 1 h prior to UV-irradiation. Cells were 10J/m² UVC-irradiated, followed by incubation for indicated time periods in media containing CHX. Whole cell lysates were resolved by 6% SDS-PAGE gel and transferred to PVDF membrane. RNA

polymerase II in 'elongation mode' (RNA polIIo) was detected with H5 (CTD-Ser2/5-P) antibody.

Ubiquitin pull-down assay. Crude lysates were prepared from mock transfected or the 6×his-tagged ubiquitin (His×6-ubiquitin) transfected HEK293T cells; the cells were 10J/m² UVC irradiated, followed by 1 h incubation. The extracts were immunoprecipitated with agarose-conjugated anti-His×6-tag antibody. Ubiquitinated RNA polIIo was detected by H5 antibody.

Small RNA interference (siRNA) experiments. *UVSSA* and *XPA* targeting siRNA oligos were purchased from *Nippon EGT* (the siRNA oligo sequences can be obtained from the companies web site). A mixture of three different siRNA oligos designed for each gene in different regions was used for all experiments unless otherwise noted. Individual siRNA oligos were also used for the experiments presented in

Supplementary Fig. 4. siRNA transfection was performed using X-tremeGENE (Roche) transfection reagent according to the manufacturer's instruction. In typical experiments, 10nM of siRNA oligos were transfected in suspension, termed 'reverse transfection', followed by one additional transfection cycle 24 h after the first transfection (double transfection). Experiments were performed 72 h after the first siRNA transfection. Knockdown efficiencies were confirmed by western blot.

Lentivirus production. Human *UVSSA* cDNA was cloned in frame with C-terminal V5-tag into pLenti6/V5-D-TOPO (Invitrogen) to generate plenti6/*UVSSA*-V5; the truncation and amino acid substitution mutants were generated from plenti6/*UVSSA*-V5 by site-directed PCR mutagenesis using specific primer sets

(primer sequences are available from T.O. upon request), PrimeSTAR HS high fidelity DNA polymerase (TaKaRa Co. Ltd.), and *DpnI* restriction enzyme (New England Biolabs Inc.). For lentivirus production, 293FT cells were transfected with *UVSSA* plasmids together with ViraPower Packaging Mix (Invitrogen) containing pLP1, pLP2 and pLP/VSVG using Lipofectamine 2000 (Invitrogen). Viral particles were collected 48 h after transfection and concentrated using PEG-it Virus Precipitation Solution (System Biosciences).

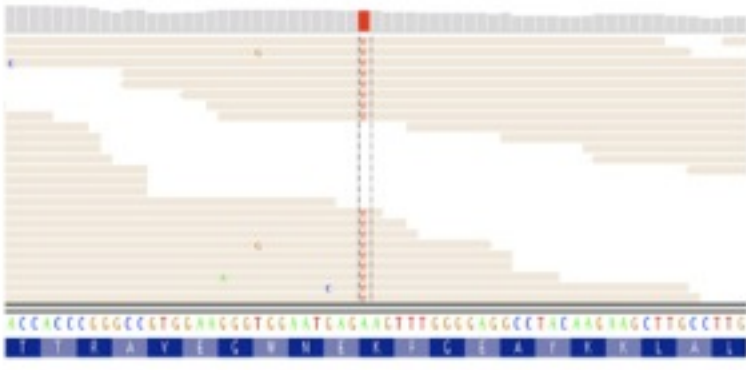
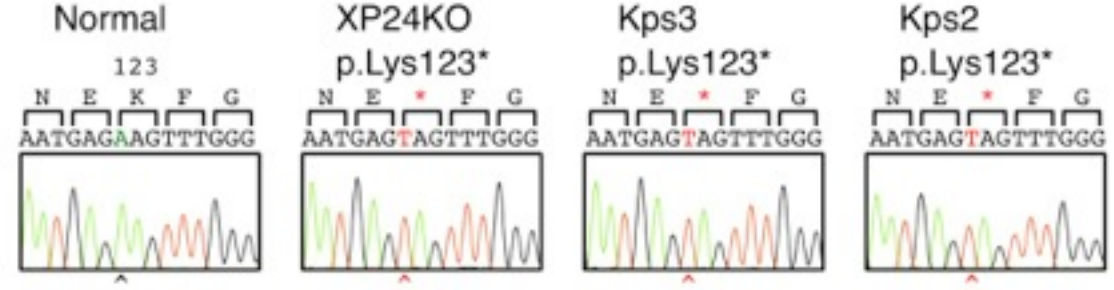
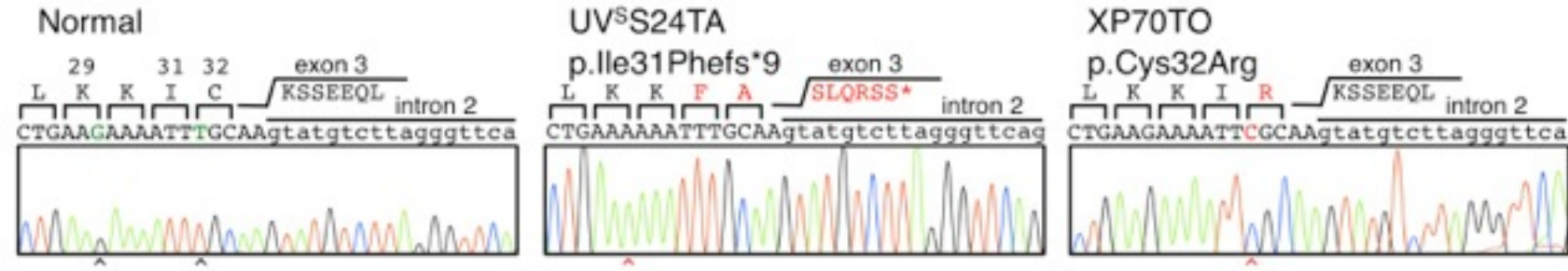
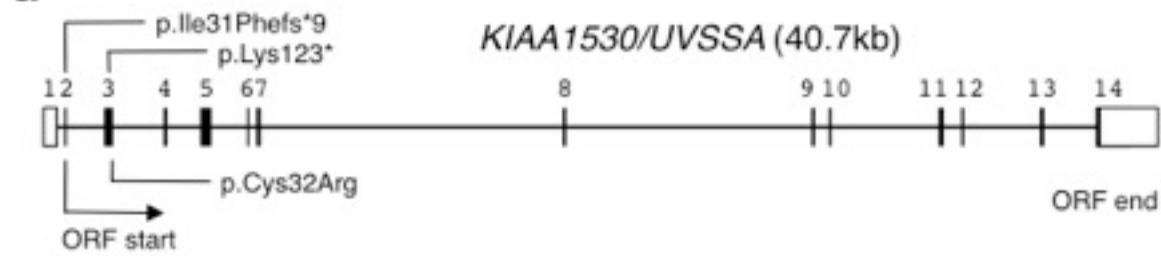
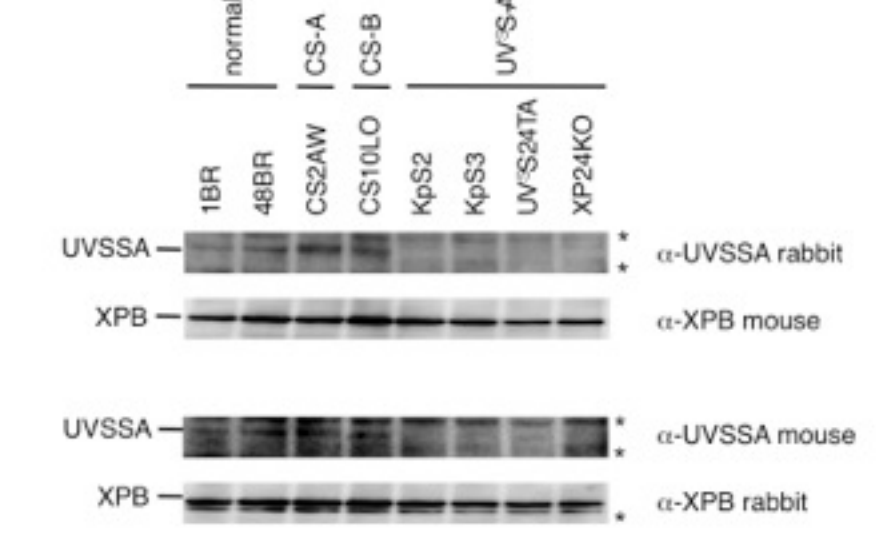
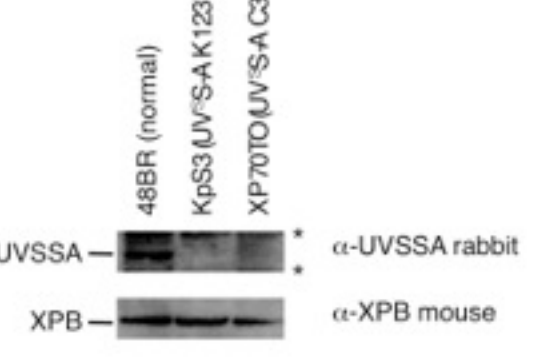
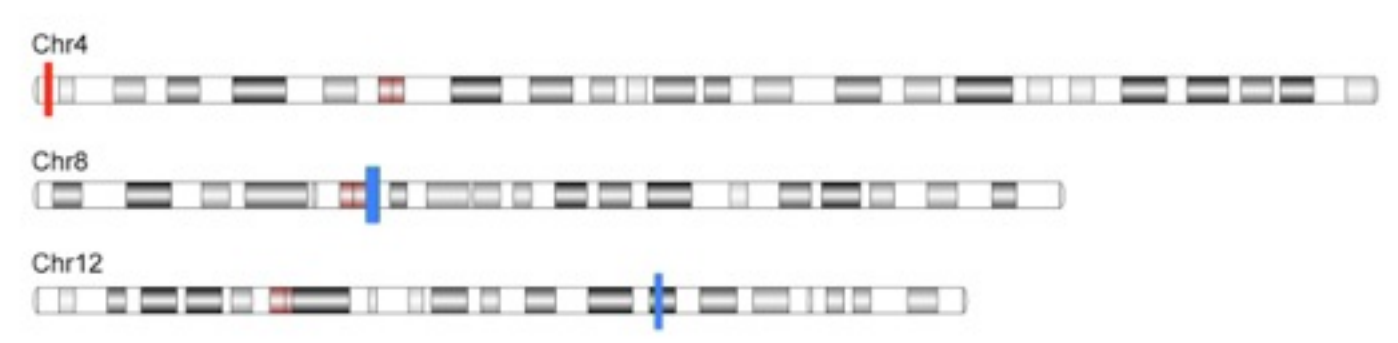
Cell-lines and culture. The following cell lines were used for this study: 48BR and 1BR, normal human primary fibroblasts; Kps2, Kps3, XP24KO, UV^SS24TA, primary fibroblasts from UV^SS-A patients; XP70TO, primary fibroblast from a mild XP-patient; CS2AW, primary fibroblast from CS-A patient; CS10LO, primary fibroblast from CS-B patient; XP15BR primary fibroblasts from XP-A patient; 293T and 293FT, human embryonic kidney HEK293T lines. All cells were maintained in DMEM (WAKO) supplemented with 10% fetal calf serum (FCS, Hyclone) and antibiotics, unless otherwise noted.

REFERENCES

1. Spivak, G. UV-sensitive syndrome. *Mutat Res* **577**, 162-9 (2005).
2. Itoh, T., Fujiwara, Y., Ono, T. & Yamaizumi, M. UVs syndrome, a new general category of photosensitive disorder with defective DNA repair, is distinct from xeroderma pigmentosum variant and rodent complementation group I. *Am J Hum Genet* **56**, 1267-76 (1995).
3. Fujiwara, Y., Ichihashi, M., Kano, Y., Goto, K. & Shimizu, K. A new human photosensitive subject with a defect in the recovery of DNA synthesis after ultraviolet-light irradiation. *J Invest Dermatol* **77**, 256-63 (1981).
4. Itoh, T., Ono, T. & Yamaizumi, M. A new UV-sensitive syndrome not belonging to any complementation groups of xeroderma pigmentosum or Cockayne syndrome: siblings showing biochemical characteristics of

- Cockayne syndrome without typical clinical manifestations. *Mutat Res* **314**, 233-48 (1994).
5. Spivak, G. *et al*. Ultraviolet-sensitive syndrome cells are defective in transcription-coupled repair of cyclobutane pyrimidine dimers. *DNA Repair (Amst)* **1**, 629-43 (2002).
 6. Hanawalt, P.C. & Spivak, G. Transcription-coupled DNA repair: two decades of progress and surprises. *Nat Rev Mol Cell Biol* **9**, 958-70 (2008).
 7. Nardo, T. *et al*. A UV-sensitive syndrome patient with a specific CSA mutation reveals separable roles for CSA in response to UV and oxidative DNA damage. *Proc Natl Acad Sci U S A* **106**, 6209-14 (2009).
 8. Horibata, K. *et al*. Complete absence of Cockayne syndrome group B gene product gives rise to UV-sensitive syndrome but not Cockayne syndrome. *Proc Natl Acad Sci U S A* **101**, 15410-5 (2004).
 9. Cleaver, J.E. & Thomas, G.H. Clinical syndromes associated with DNA repair deficiency and enhanced sun sensitivity. *Arch Dermatol* **129**, 348-50 (1993).
 10. Itoh, T., Linn, S., Ono, T. & Yamaizumi, M. Reinvestigation of the classification of five cell strains of xeroderma pigmentosum group E with reclassification of three of them. *J Invest Dermatol* **114**, 1022-9 (2000).
 11. Ng, S.B. *et al*. Targeted capture and massively parallel sequencing of 12 human exomes. *Nature* **461**, 272-6 (2009).
 12. Kawada, A., Satoh, Y. & Fujiwara, Y. Xeroderma pigmentosum complementation group E: a case report. *Photodermatol* **3**, 233-8 (1986).
 13. Stefanini, M. *et al*. Genetic heterogeneity of the excision repair defect associated with trichothiodystrophy. *Carcinogenesis* **14**, 1101-5 (1993).
 14. Mayne, L.V. & Lehmann, A.R. Failure of RNA synthesis to recover after UV irradiation: an early defect in cells from individuals with Cockayne's syndrome and xeroderma pigmentosum. *Cancer Res* **42**, 1473-8 (1982).
 15. Limsirichaikul, S. *et al*. A rapid non-radioactive technique for measurement of repair synthesis in primary human fibroblasts by incorporation of ethynyl deoxyuridine (EdU). *Nucleic Acids Res* **37**, e31 (2009).
 16. Nakazawa, Y., Yamashita, S., Lehmann, A.R. & Ogi, T. A semi-automated non-radioactive system for measuring recovery of RNA synthesis and unscheduled DNA synthesis using ethynyluracil derivatives. *DNA Repair (Amst)* **9**, 506-16 (2010).
 17. Kelley, L.A. & Sternberg, M.J. Protein structure prediction on the Web: a case study using the Phyre server. *Nat Protoc* **4**, 363-71 (2009).
 18. Lohi, O., Poussu, A., Mao, Y., Quijcho, F. & Lehto, V.P. VHS domain -- a longshoreman of vesicle lines. *FEBS Lett* **513**, 19-23 (2002).
 19. Dikic, I., Wakatsuki, S. & Walters, K.J. Ubiquitin-binding domains - from structures to functions. *Nat Rev Mol Cell Biol* **10**, 659-71 (2009).
 20. Ren, X. & Hurley, J.H. VHS domains of ESCRT-0 cooperate in high-avidity binding to polyubiquitinated cargo. *EMBO J* **29**, 1045-54 (2010).
 21. Ito, S. *et al*. XPG stabilizes TFIIH, allowing transactivation of nuclear receptors: implications for Cockayne syndrome in XP-G/CS patients. *Mol Cell* **26**, 231-43 (2007).
 22. Fouteri, M., Vermeulen, W., van Zeeland, A.A. & Mullenders, L.H. Cockayne syndrome A and B proteins differentially regulate recruitment of

- chromatin remodeling and repair factors to stalled RNA polymerase II in vivo. *Mol Cell* **23**, 471-82 (2006).
23. Bregman, D.B. *et al* UV-induced ubiquitination of RNA polymerase II: a novel modification deficient in Cockayne syndrome cells. *Proc Natl Acad Sci U S A* **93**, 11586-90 (1996).
 24. Rockx, D.A. *et al* UV-induced inhibition of transcription involves repression of transcription initiation and phosphorylation of RNA polymerase II. *Proc Natl Acad Sci U S A* **97**, 10503-8 (2000).
 25. Anindya, R., Aygun, O. & Svejstrup, J.Q. Damage-induced ubiquitylation of human RNA polymerase II by the ubiquitin ligase Nedd4, but not Cockayne syndrome proteins or BRCA1. *Mol Cell* **28**, 386-97 (2007).
 26. Starita, L.M. *et al* BRCA1/BARD1 ubiquitinate phosphorylated RNA polymerase II. *J Biol Chem* **280**, 24498-505 (2005).
 27. Kleiman, F.E. *et al* BRCA1/BARD1 inhibition of mRNA 3' processing involves targeted degradation of RNA polymerase II. *Genes Dev* **19**, 1227-37 (2005).
 28. Takagi, Y. *et al* Ubiquitin ligase activity of TFIIF and the transcriptional response to DNA damage. *Mol Cell* **18**, 237-43 (2005).
 29. Spivak, G. & Hanawalt, P.C. Host cell reactivation of plasmids containing oxidative DNA lesions is defective in Cockayne syndrome but normal in UV-sensitive syndrome fibroblasts. *DNA Repair (Amst)* **5**, 13-22 (2006).
 30. D'Errico, M. *et al* The role of CSA in the response to oxidative DNA damage in human cells. *Oncogene* **26**, 4336-43 (2007).
 31. Li, H. & Durbin, R. Fast and accurate short read alignment with Burrows-Wheeler transform. *Bioinformatics* **25**, 1754-60 (2009).
 32. DePristo, M.A. *et al* A framework for variation discovery and genotyping using next-generation DNA sequencing data. *Nat Genet* **43**, 491-8 (2011).
 33. McKenna, A. *et al* The Genome Analysis Toolkit: a MapReduce framework for analyzing next-generation DNA sequencing data. *Genome Res* **20**, 1297-303 (2010).
 34. Albers, C.A. *et al* Dindel: accurate indel calls from short-read data. *Genome Res* **21**, 961-73 (2011).
 35. Wang, K., Li, M. & Hakonarson, H. ANNOVAR: functional annotation of genetic variants from high-throughput sequencing data. *Nucleic Acids Res* **38**, e164 (2010).
 36. Ng, P.C. & Henikoff, S. SIFT: Predicting amino acid changes that affect protein function. *Nucleic Acids Res* **31**, 3812-4 (2003).

a Kps3 KIAA1530/UVSSA:c.367A>T**b****c****d****e****f****g****Fig.1**

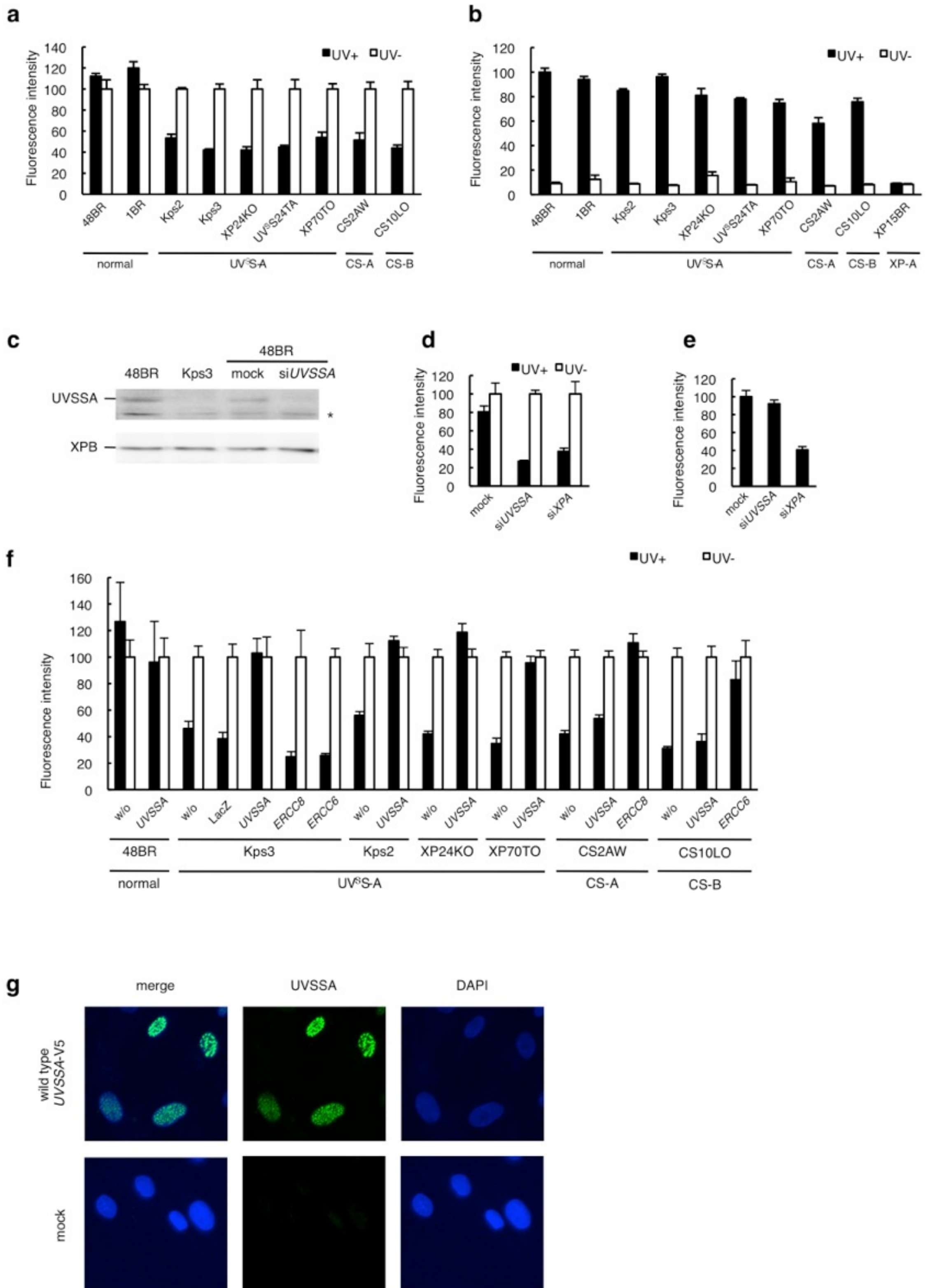


Fig.2

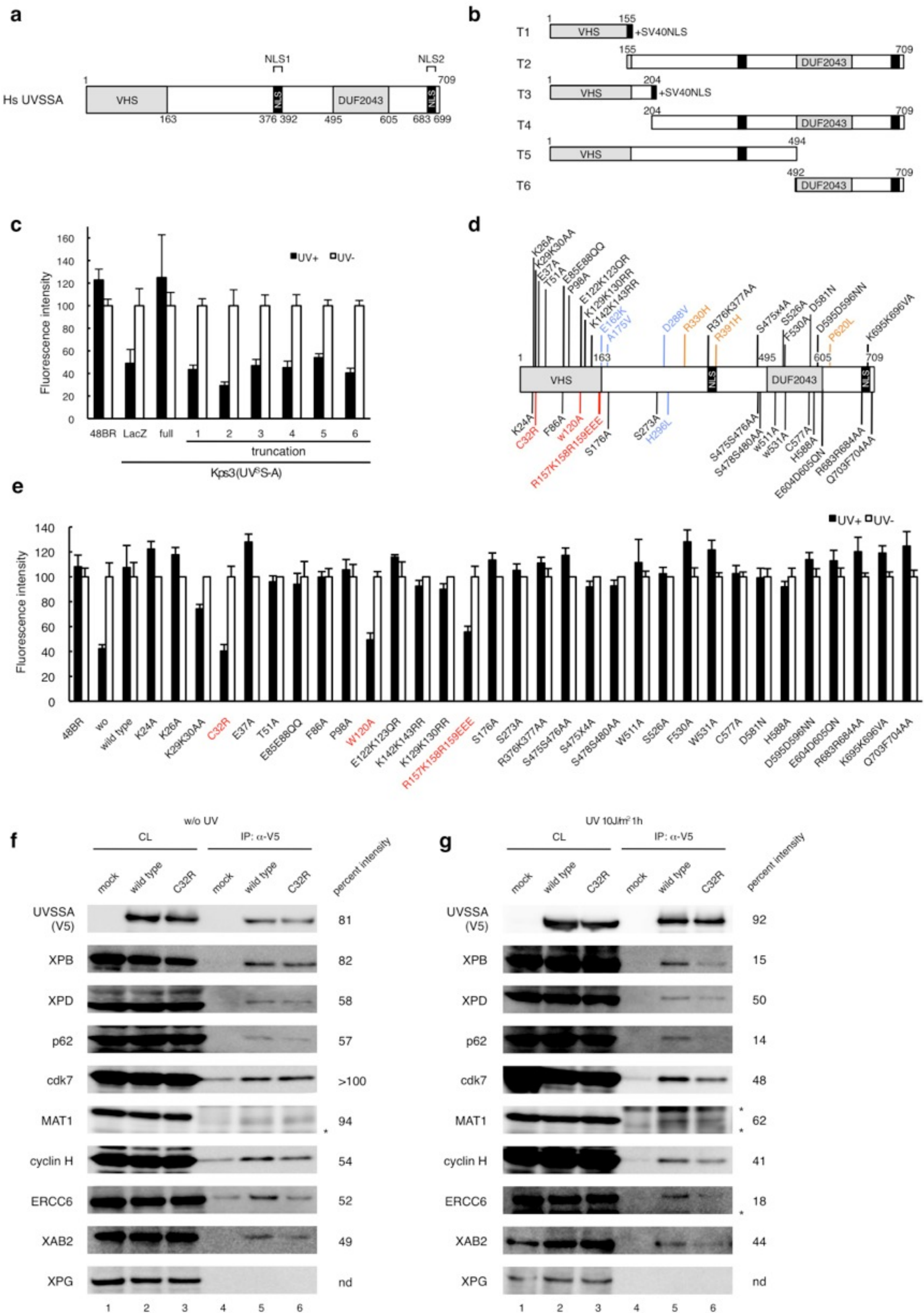


Fig.3

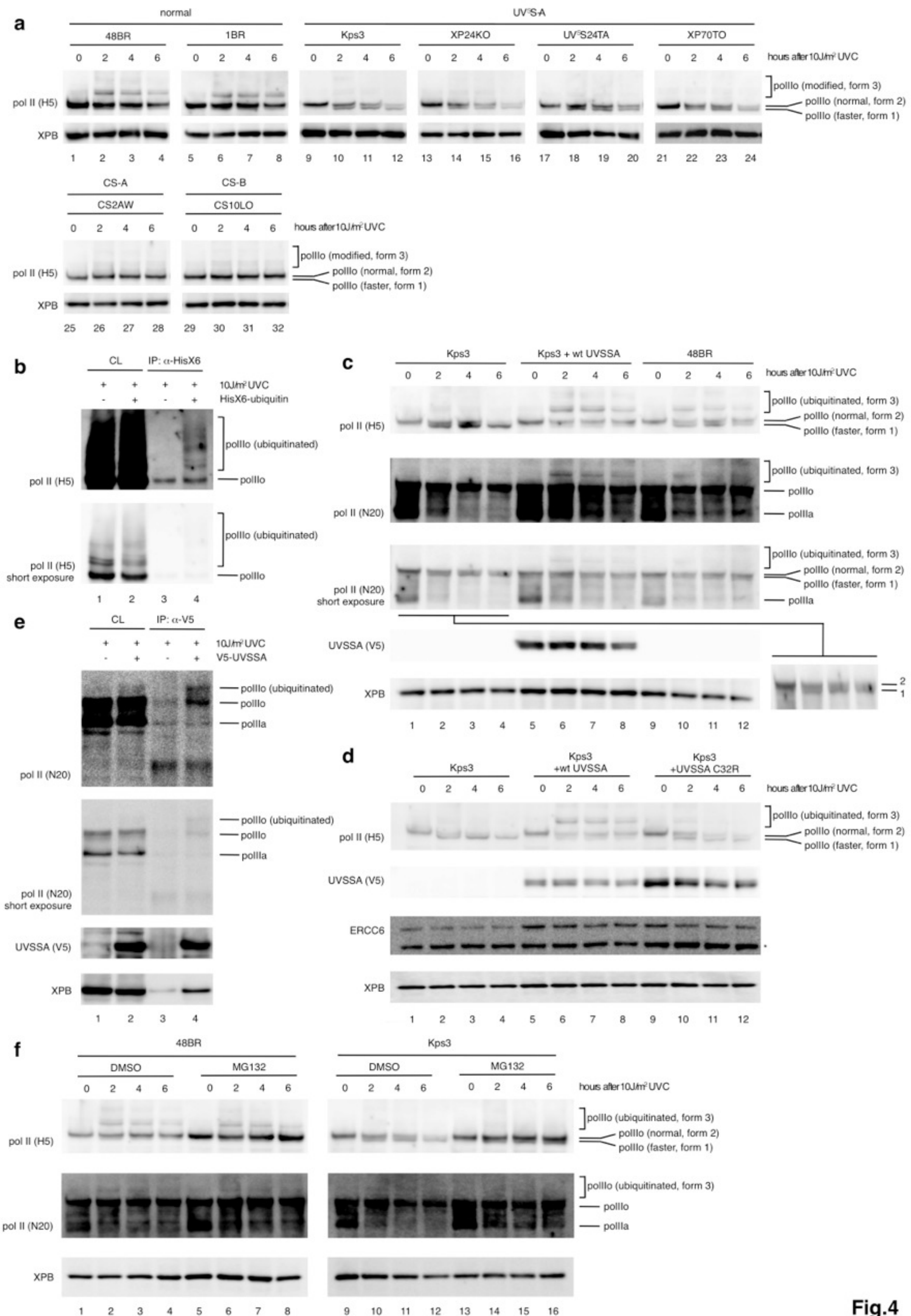


Fig.4